Experimental Testing and Analytical Modelling of Damage-Avoidance Steel Connections using HF2V Damping Devices

2009 NZSEE Conference

G.W. Rodgers

Zachry Dept. of Civil Engineering, Texas A&M Univ., College Station, Texas, and Dept. of Mechanical Engineering, Univ. of Canterbury, Christchurch, NZ.

J.B. Mander

Zachry Dept. Civil Engineering, Texas A&M Univ., College Station, Texas.

J.G. Chase

Dept. of Mechanical Engineering, Univ. of Canterbury, Christchurch, NZ.

ABSTRACT: Analytical modelling and model validation of high force-to-volume (HF2V) damping devices and a DAD non-dilating steel connection utilising these devices is presented. The 2D exterior connection design incorporates a top-hung angle for the beam-column connection and HF2V devices create a damage-free moment resisting connection. Experimental results show consistently repeatable hysteretic behaviour to 4% drift with neither stiffness nor strength degradation. The analytical model of the connection shows good agreement between experimental and model results. The rate-dependent model defines overall hysteresis using a predictor-corrector solution to the governing non-linear ODE. Based entirely on rational mechanics, the model does not require prior experimental data for empirical calibration, enabling simultaneous design of the desired connection mechanics and energy dissipation, and the device requirements.

1 INTRODUCTION

In recent research, high force-to-volume (HF2V) lead based dampers have been developed to provide large resistive forces and maintain compact outer dimensions (Rodgers et al. 2007; Rodgers et al. 2008a). These devices have been implemented into several large-scale experiments, using both jointed-precast concrete and steel beam-to-column rigid connections (Mander et al. 2009; Rodgers et al. 2008b). During these experimental investigations it has become apparent that the influence of connecting elements has a large effect on the connection rigidity and energy dissipation capacity. Specifically, any flexibility and take-up of the connecting elements reduces the displacements induced in the damper, thereby reducing the ability of the damper to efficiently dissipate energy. Therefore, to obtain the best performance it is important to minimise the connection flexibility. Despite efforts to reduce the flexibility, practical limitations on shaft and connection sizes dictate that a measure of connection flexibility will always exist and have an effect on overall behaviour. Therefore, it is of importance to develop a model that incorporates both the fundamental damper mechanics, while also incorporating the effects of connection flexibility.

Previous research has looked at overall flexibility components of steel connections and how they relate to subassembly deformation and fatigue considerations (Mander et al. 1994). Other research has investigated experimental testing and modelling the response of post-tensioned steel connections (Garlock et al. 2007; Pekcan et al. 2000), but has not investigated the use of non-linear viscous dampers within a steel frame. This paper describes a non-linear viscous damper and flexibility model, and also explains the incorporation of this model into a rocking steel connection. This overall model can be used to determine the overall connection behaviour from damper, connection and member properties, using a rational mechanics based approach.

2 TRANSIENT DAMPER MODEL

2.1 Damper Model Derivation

Consider a non-linear HF2V damper (Rodgers et al. 2007; 2008a) connected in series with a linear axial spring to give a system of the Maxwell type, schematically presented in Figure 1. The displacement across the spring is *x*, the displacement across the damper is *y*, and the total displacement across the system is *z*. The system is formulated such that *z* is a known input displacement as a function of time, and the values of *x*, *y*, and the overall system force, *F*, are calculated.

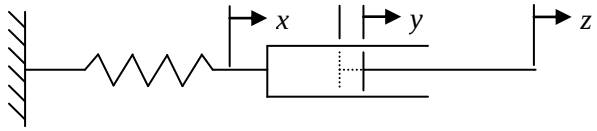

Figure 1: Schematic diagram of the damper-spring system

Due to the series nature of the system the displacements and velocities will sum, therefore:

$$x + y = z \tag{1}$$

$$\dot{x} + \dot{y} = \dot{z} \tag{1b}$$

The applied force, F_D, must also equal the spring force (Kx) and the damper force. Using the Pekcan et al (1999) model for non-linear viscous dampers:

$$F_D = \frac{x}{f_D} = C_\alpha |\dot{y}|^\alpha \operatorname{sgn}(\dot{y}) \tag{2}$$

in which f_D = the axial flexibility of the spring component of the damper assembly ($f_D = 1/K$), where K is the spring stiffness of the damper assembly; C_α = a damper constant; α = the velocity exponent; and $\dot{y}$ = the velocity across the damper.

Herein a numerical solution approach is used to solve the coupling between (1) and (2). Using backward differences, a numerical solution can be obtained from:

$$\dot{y}_{i+1} = \frac{z_{i+1} - z_i + f_D F_i}{\Delta t + f_D C_\alpha^{(1/\alpha)} |F_{i+1}|^{1-1/\alpha}} \tag{3}$$

$$F_{i+1} = C_\alpha |\dot{y}_{i+1}|^\alpha \operatorname{sgn}(\dot{y}_{i+1}) \tag{4}$$

The coupling of (3) and (4) requires that these equations must be solved in a predictor-corrector sense. For the initial step the first predictor of force is given by:

$$F_1 = \frac{z_1}{f_D} \tag{5}$$

And for all subsequent steps the following has been found to be a suitable predictor:

$$F_{i+1} = F_i + \frac{\Delta t}{f_D}(2\dot{x}_i - \dot{x}_{i-1}) \tag{6}$$

From this solution the value of the system force on each successive time step can be obtained. This result is then used to give the value of the spring displacement, *x*, as well as the damper displacement, *y*, and their derivatives.

This predictor-corrector approach provides an accurate solution to the system equations (without iteration) as long as the time step is kept small, as it is only conditionally stable. Although the solution method presented in (3) and (4) provides accurate results and is relatively easy to implement, accuracy can be improved if they are solved iteratively. Providing the time step used is appropriately small, convergence is rapid.

2.2 **Damper Model Validation**

Experimental results of a velocity-dependent HF2V device are now used to validate the above force-displacement analytical model. The HF2V device was tested at a range of different velocities in a DARTEC^{TM} universal testing machine to characterize the damper constant, C_α, and the velocity exponent, α. The device velocity exponent was determined, as presented in Mander et al. (2009) and has also been characterized in a previous study using a different HF2V device (Rodgers et al. 2008a). Both studies give a velocity exponent in the range of $\alpha = 0.11$ to 0.12, which is within the range found for much larger lead extrusion damping devices (Cousins and Porritt 1993).

Figure 2 presents the experimental tests at two different input sine-wave frequencies of 0.01 and 0.0025 Hz along with the analytical model of the HF2V device response. When applying the model in (1) to (6), the following parameters were used, $\alpha = 0.12$, $C_\alpha = 170$, $f_D = 3.3 \times 10^{-3}$ mm/kN. Figure 2 indicates that good agreement exists between the experimental behaviour and the model prediction.

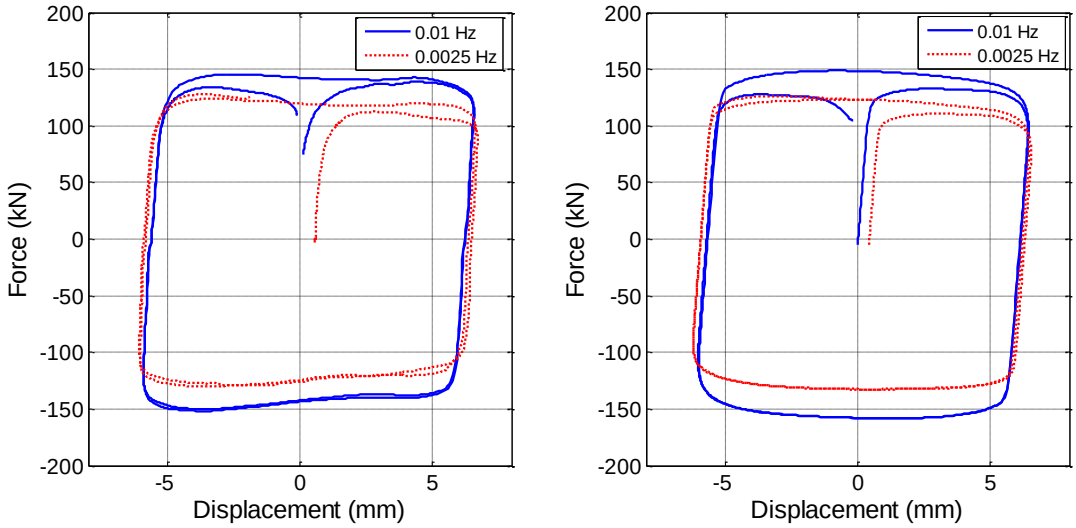

a) Experimental Results *b) Model Results*

Figure 2: Comparison of experimental and model results

3 **ROTATIONAL FORMULATION FOR HF2V DAMPERS IN BEAM-COLUMN JOINTS**

3.1 **Structural Flexibility**

Recent research has investigated using HF2V devices in a steel beam-to-column connection of the variety presented in Figure 3 (Mander et al. 2009). The top-hung steel flange (beam) connection can be modelled as a rotational version of the linear (translational) damper model presented above. The presence of the beam and column in effect provide additional sources of flexibility. Thus, in extending the behavioural model to capture the rotational effects the structural elements must first be considered, without the displacement/rotation contributions from the damper displacement, y. If the damper is locked, such that $y = 0$, then the flexibility contributions of the structural elements can be determined.

The total displacement at the top of the column shown in Figure 3 becomes a combination of displacement contributions from the column, the beam, and the connection rotation due to damper connection flexibility and angle flexibility. This relationship can be written as:

$$\Delta_T = \Delta_c + \Delta_b + \Delta_x \tag{7}$$

where Δ_T = the total displacement due to all flexibility effects; Δ_c = the displacement contribution from column flexibility; Δ_b = the contribution from beam flexibility; and Δ_x = the contribution due to the

connection rotation as a result of damper connection and top angle flexibility, and shear deformation of the column panel zone.

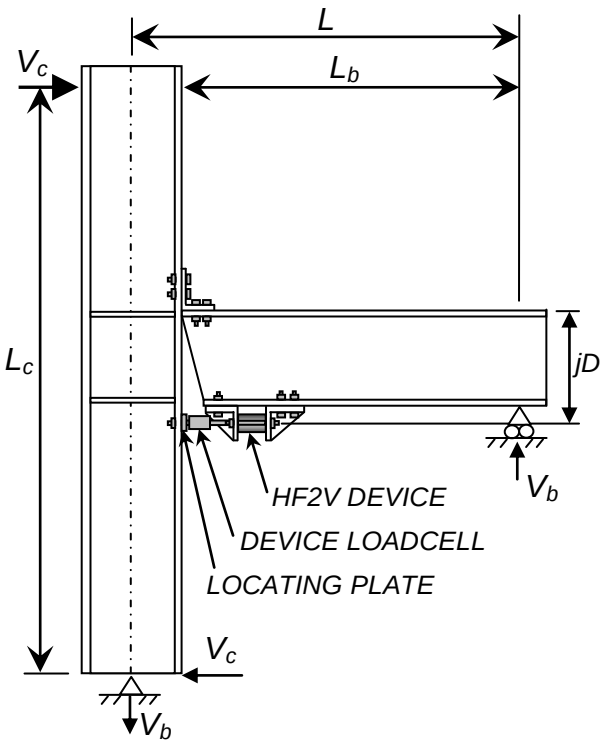

Figure 3: Schematic diagram of steel beam-to-column subassemblage with HF2V device

Each of these individual contributions can be individually defined based on well-known structural mechanics. The drift angle due to column deflection is:

$$\theta_C = \frac{V_C L_C^2}{12EI_C} \tag{8}$$

where L_c = defined as the column height, as shown in Figure 3; and EI_c = the column rigidity.

Similarly, the beam rotation, θ_b, due to the beam shear is given as:

$$\theta_b = \frac{V_b L_b^2}{3EI_b} \tag{9}$$

where L_b = the clear beam length, as shown in Figure 3; and EI_b = the beam rigidity. From moment equilibrium of the subassembly, the beam shear can be related to the column shear, and this relationship can then be used to define the beam rotation in terms column shear:

$$\theta_b = V_C \frac{L_b^2}{3EI_b} \frac{L_c}{L} \tag{10}$$

where L = the distance from the column centerline to the beam strut location, as shown in Figure 3.

During elastic deformation the beam rotation will be equal to the column rotation, so no further transformation is required. The rotation of the column due to the overall joint flexibility components, f_D, can be determined based on simple geometric transformations. For a given damper force, F_D, the displacement across the connecting elements, x, is given by (2) ($x = f_D F_D$). From this displacement, x, the column rotation can be defined as:

$$\theta_x = \frac{f_D F_D}{jD} \tag{11}$$

where f_D = the flexibility associated with the damper connections, shear deformation of the panel zone, and deflection of the top angle; jD = the internal lever arm between the top angle/flange-hung connection and the line of the re-action of the damper, as shown schematically in Figure 3.

Moment equilibrium of the beam requires:

$$F_D = \frac{V_b L_b}{jD} \tag{12}$$

By re-arranging, the overall column shear as a function of the damper force is:

$$V_C = F_D \frac{jD}{L_C} \frac{L}{L_b} \tag{13}$$

Substituting (13) into (11) gives the column rotation as a function of column base-shear:

$$\theta_x = V_C \frac{f_D L_b L_c}{(jD)^2 L} \tag{14}$$

Summing these components gives total elastic structural drift, θ_S, as a function of column base-shear:

$$\theta_S = V_c f_\theta \tag{15}$$

where f_θ = the total rotational elastic flexibility, defined as:

$$f_\theta = f_{\theta c} + f_{\theta b} + f_{\theta x} \tag{16}$$

where the results of (8), (10), and (14) are divided by the column base-shear to obtain the flexibility and substituted into (16) to give:

$$f_\theta = \frac{L_C^2}{12EI_c} + \frac{L_C L_b^2}{3L\,EI_b} + \frac{f_D L_b L_C}{(jD)^2 L} \tag{17}$$

where f_D = the connection flexibility. This flexibility can be analysed from rational mechanics, FEM studies, or inferred from experimental results.

3.2 **Numerical Implementation**

The model terms for the structural system have a simple analogy to the translational damper system model that was previously presented and validated above. The flexibility terms, as expressed in (15) and (17) are analogous to the spring flexibility, f_D, in the simple translational model. Likewise, the rotation component from damper motion is analogous to the damper term, y, in the linear damper model. Therefore, the numerical predictor-corrector solution can be modified to utilise these common facets, and thus be re-formulated to define a relationship between joint rotation and column base-shear. From (6) it follows that the predictor step is:

$$V_{c,i+1} = V_{c,i} + \frac{\Delta t}{f_\theta}\left(2\dot{\theta}_{S,i} - \dot{\theta}_{S,i-1}\right) \tag{18}$$

During the initial few time-steps, a different approximation must be used, as the backward difference values may not be available for application. During these initial few steps, the base-shear can be obtained by considering that initial deformation will be governed by the elastic regime only, thus:

$$V_{C,i} = \frac{\theta_{z,i}}{f_\theta} \tag{19}$$

where θ_z = the total known input rotation to the system; and f_θ = the total elastic flexibility as defined previously in (17). The corrector step takes a very similar form to that previously presented for the simplified model presented in (3) and (4), and is defined:

$$\dot{\theta}_{y,i} = \frac{\theta_{z,i+1} - \theta_{z,i} + \theta_{S,i}}{\Delta t + f_\theta \, C_\theta^{\,1/\alpha} \left| V_{C,i} \right|^{1-1/\alpha}} \tag{20}$$

This new value of $\dot{\theta}_{y,i}$ can then be used as a corrector step, to re-calculate the system force, $V_{c,i}$, using:

$$V_{c,i} = C_\theta \left| \dot{\theta}_{y,i} \right|^\alpha \operatorname{sgn}\left(\dot{\theta}_{y,i} \right) \tag{21}$$

As before, this system of equations can be iterated to converge onto a solution within each time-step. Alternatively, this predictor-corrector approach can be used without iteration, with the limitation that it is only conditionally stable and must utilize a sufficiently fine time-step.

4 BEAM-COLUMN JOINT MODEL VALIDATION

As previously described, a steel beam-column connection with top-hung angle connection was used as the experimental specimen, as shown schematically in Figure 3. The 2D specimen utilized a cut back beam end to allow positive and negative (gap-opening and closing) joint rotations. Basic specimen dimensions, as defined in Figure 3, were L_c = 2 m, L = 1.5 m, using member sections 360UB44.7 and 310UC15 for the beam and column respectively. The HF2V device utilised was the same as that previously characterized, as shown in Figure 2. More specific specimen dimensions, different configurations, design considerations, and hysteresis results are presented in Mander et al (2009).

Figure 4a presents the experimentally observed behaviour under reversed cyclic loading to drift amplitudes of 0.25, 0.5, 1, 2, 3, and 4%. Figure 4b shows the modelled results using (18) to (21). Although good agreement between the observed and modeled results is evident, several points should be noted.

5 DISCUSSION

The experimental results presented in Figure 4a indicate that the model will require a modification to the overall flexibility value to represent the asymmetry in the stiffness values. The flexibility component associated with of bending of the top-angle connection, is dependent on the assumed boundary conditions. The inferred pull-off displacement between the angle and the column face is determined from local joint potentiometer readings. This data indicates that the displacement is well modelled by the assumptions that the angle acts with fixed pinned boundary conditions under joint closing, but acts more like fixed-fixed boundary conditions during joint opening. Therefore, the model is modified such that the flexibility value for the angle is dependent on the loading regime.

If the column base-shear is positive and the displacement is increasing (increase in joint closing drift) or the column base-shear is negative, and the displacement is decreasing (increase in joint opening drift), then the angle flexibility value is modified to indicate fixed-pinned boundary conditions. If the base-shear is positive, but the displacement is decreasing (decrease in joint closing drift), or the base-shear is negative and the displacement is increasing (decrease in joint opening drift), then the angle flexibility is modified to indicate a fixed-fixed condition. The analytical model results using this approach and flexibilities calculated from the rotational model is presented in Figure 4b. This simple addition of heuristics based on the deformation regime of the top angle bracket gives good agreement with the experimental results, as shown in Figure 4b. The transition of stiffness values is done using a hyperbolic tangent function for a smooth transition, to avoid large stiffness changes across a time-step, which could destabilize the numerical solution.

It is evident in Figure 4 that the variable stiffness is an important consideration to capture the different reaction mechanisms that are present in the experimental results. Overall, the model and experimental results show good agreement. However, the experimental results show a slight bi-linear behavior that is attributed to additional friction and binding of the shaft due to the lateral load induced. This lateral load is due to the joint motion, which is an arc about the rocking edge, whereas the shaft itself only has the ability to move in a linear path. Therefore, some bending will be induced within the shaft which may produce a variable friction force which contributes to the overall column base-shear. The use of a clevis attachment in future applications should minimise these effects and, as such, provide more predictable results.

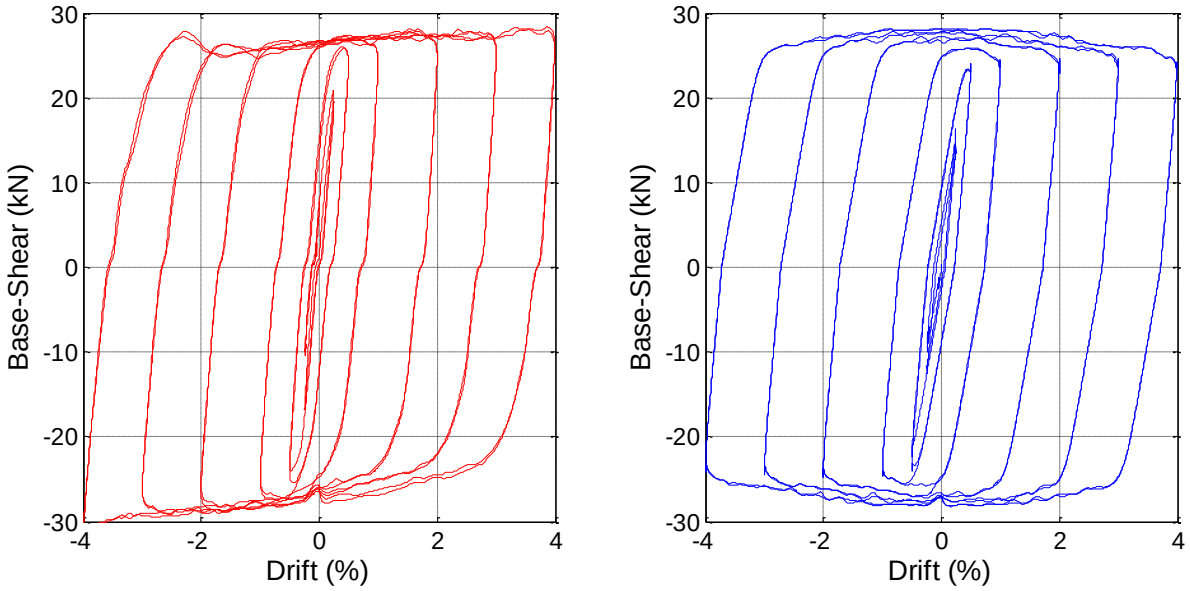

a) Experimental Results *b) Model Results*

Figure 4: Comparison of experimental and model results for overall subassembly

Another key aspect of the joint behaviour that is evident in the results of Figure 4 is the large influence that the angle flexibility has on the overall performance. It is advantageous to have a high initial stiffness and low yield drift, for a given yield force. The angle reaction regime has a large influence on the overall elastic stiffness of the subassembly. Therefore, it has become evident that to stiffen the connection the angle connection is a primary consideration. It is therefore advisable that in future connections the top-hung angle would be modified to incorporate a split-tee connection (WT-shape). The angle used in the experiment was equivalent to a L6 x 6 x ½ and could be easily replaced by a WT shaped connection, such as the WT6x39.5. The flange would then be bolted to the column face and the web would be used for connection to the beam flange.

The use of the clevis attachments would maintain only axial force in the damper and eliminate the bi-linear component seen in Figure 4. This connection detailing should result in a higher initial elastic stiffness (reduced flexibility), lower yield drift, and a more rigid structure. It is advantageous to have this higher initial stiffness to reduce structural drifts. A schematic diagram of the proposed new experimental set-up, using both the clevis damper attachments and split-tee connection is presented in Figure 5.

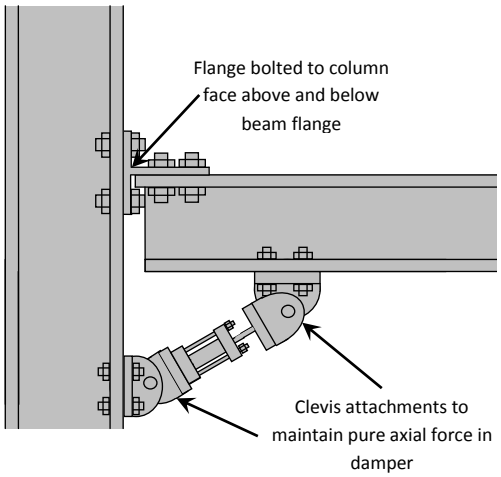

Figure 5: Proposed subassembly design incorporating different connection detail and damper clevis

6 CONCLUSIONS

A simple damper model was presented that accounts for connection flexibility and velocity-dependence of the damper. The damper model was validated against experimental data, and shows good agreement. The damper model can then be extended to a rotational base-shear to drift relationship, by accounting for structural member flexibility and geometric transformations. The approach, based entirely on rational mechanics, provides a good model of joint hysteresis, without empirically determined constants. A slight asymmetry is present in the hysteresis results, due to different reaction mechanisms of the top angle connection.

ACKNOWLEDGEMENTS:

The modelling work presented herein was developed while the first author was resident of Texas A&M University on a Fulbright-EQC Graduate Award. This support, and the support of the Tertiary Education Commission through the Bright Futures scheme, is gratefully acknowledged.

REFERENCES:

Cousins, W. J., and Porritt, T. E. (1993). "Improvements to lead-extrusion damper technology." *Bulletin of the New Zealand National Society for Earthquake Engineering*, 26(3), 342-348.

Garlock, M. M., Sause, R., and Ricles, J. M. (2007). "Behavior and design of posttensioned steel frame systems." *Journal of Structural Engineering*, 133(3), 389-399.

Mander, J. B., Chen, S. S., and Pekcan, G. (1994). "Low-cycle fatigue behavior of semi-rigid top-and-seat angle connections." *Engineering Journal*, 31(3), 111-122.

Mander, T. J., Rodgers, G. W., Chase, J. G., Mander, J. B., and MacRae, G. A. (2009). "A Damage Avoidance Design Steel Beam-Column Moment Connection Using High-Force-To-Volume Dissipators." *ASCE Journal of Structural Engineering*, In press.

Pekcan, G., Mander, J. B., and Chen, S. S. (1999). "Fundamental considerations for the design of non-linear viscous dampers." *Earthquake Engineering and Structural Dynamics*, 28(11), 1405-1425.

Pekcan, G., Mander, J. B., and Chen, S. S. (2000). "Experiments on steel MRF building with supplemental tendon system." *Journal of Structural Engineering*, 126(4), 437-444.

Rodgers, G. W., Chase, J. G., Mander, J. B., Leach, N. C., and Denmead, C. S. (2007). "Experimental development, tradeoff analysis and design implementation of high force-to-volume damping technology." *Bulletin of the New Zealand Society for Earthquake Engineering*, 40(2), 35-48.

Rodgers, G. W., Mander, J. B., Chase, J. G., Dhakal, R. P., Leach, N. C., and Denmead, C. S. (2008a). "Spectral analysis and design approach for high force-to-volume extrusion damper-based structural energy dissipation." *Earthquake Engineering & Structural Dynamics*, 37(2), 207-223.

Rodgers, G. W., Solberg, K. M., Mander, J. B., Chase, J. G., Bradley, B. A., Dhakal, R. P., and Li, L. (2008b). "Performance Of A Damage-Protected Beam-Column Subassembly Utilizing External HF2V Energy Dissipation Devices." *Earthquake Engineering & Structural Dynamics*, 37(13), 1549-1564